This paper is published in Langmuir 37, 348-356 (2021)
doi/10.1021/acs.langmuir.0c02945

Fabrication of transparent and microstructured superhydrophobic substrates using additive manufacturing

Ahmed Aldhaleai and Peichun Amy Tsai*

Mechanical Engineering, University of Alberta, Edmonton, Alberta T6G 1H9, Canada

E-mail: peichun.amy.tsai@ualberta.ca

Abstract

We report facile one- and two-step processes for the fabrication of transparent ultra-hydrophobic surfaces and 3D-printed superhydrophobic (SH) microstructures, respectively. In the one-step method, polydimethylsiloxane (PDMS) solution is treated thermally at 350°C for 4 hours, while PDMS soot is generated and deposited on a glass slide to obtain a transparent SH surface without further chemical modification. For the two-step approach, SH surfaces are obtained by incorporating a 3D-printing technique with a convenient hydrophobic coating method. Herein, we first 3D-print microstructured substrates with particular surface parameters, which are designed to facilitate a stable gas-trapping, Cassie-Baxter (CB) wetting state based on a thermodynamic theory. We subsequently coat the 3D-printed microstructures with candle soot (CS) or Octadecyltrichlorosilane (OTS) solution to make superhydrophobic surfaces with mechanical durability. These surfaces exhibit an ultrahigh static water contact angle (CA, $\theta \simeq 158 \pm 2°$ and $\theta \simeq 147 \pm 2°$ for the CS and OTS coating, respectively) and a low roll-off angle for water droplets. Both static and dynamic (in terms of the advancing and receding) contact angles of a water droplet on the fabricated SH surfaces are in good agreement with the theoretical prediction of Cassie-Baxter contact angles. Furthermore, after a one-year-long shelf time, the SH substrates fabricated sustain good superhydrophobicity after ultrasonic water treatment and against several chemical droplets. All these methods are simple, cost-effective, and highly efficient processes. The processes, design principle, and contact angle measurements presented here are useful for preparing transparent and superhydrophobic surfaces using additive manufacturing, which enables large-scale production and promisingly expands the application scope of utilizing self-cleaning superhydrophobic material.

Introduction

Superhydrophobic (SH) surfaces consist of hydrophobic material with micro- and nano-scale roughness or structures, with a static water contact angle (CA) greater than 150°,[1] and have attracted significant interest due to their importance in both scientific research and practical applications. Many natural living systems such as lotus leaves,[2–4] ramee leaves,[5] rice leaves,[6] and butterfly wings[7] exhibit superhydrophobicity, giving rise to self-cleaning,[8–10] water or oil repellency,[11,12] drag-reduction,[13] anti-icing,[14] anti-fouling,[15] and many other appealing applications. These applications have inspired many researchers to develop artificial SH surfaces with biomimetic structures of an ultrahigh CA, but ultralow water adhesion.

The wettability of SH surfaces strongly depends on both the surface geometry (e.g., surface roughness and structures) and chemical nature (e.g., surface free energy). Therefore, most studies have mainly focused on either altering the chemical

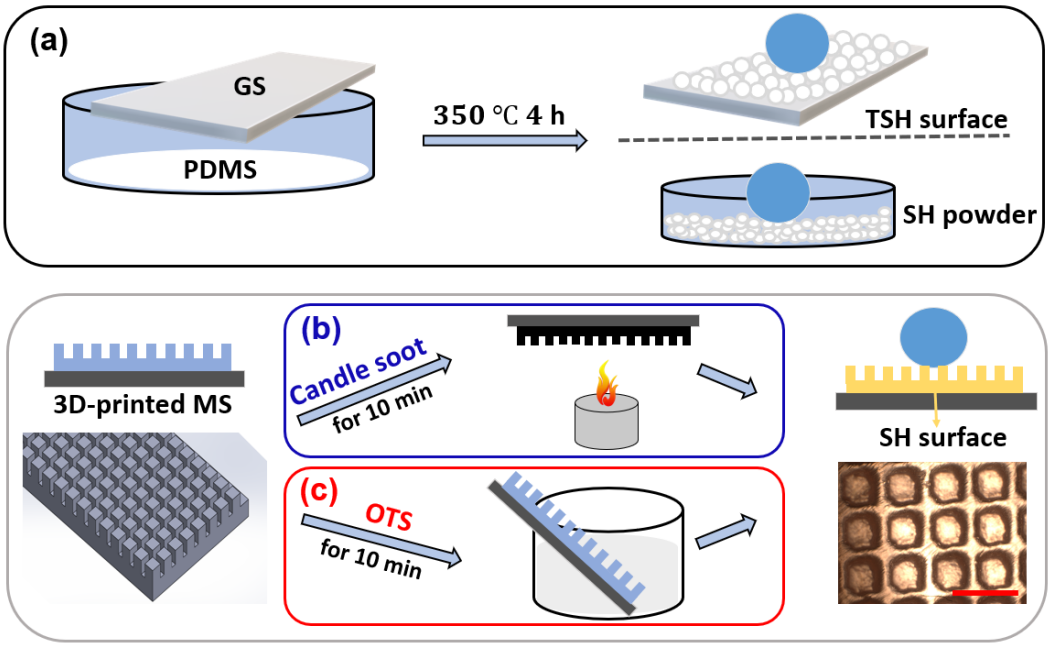

Figure 1. Schematic of the three processes for preparing superhydrophobic (SH) surfaces. In (a), transparent SH surface and SH powder were prepared using a one-step heating procedure of liquid PDMS at 350°C for four hours. When the liquid PDMS is heated, it decomposes and generates soot, depositing on a glass slide (GS) to form a transparent SH surface. The remaining silicon powder left in the pyrex also shows SH properties for water droplets. In (b) and (c), using two-step processes, we first 3D-printed microstructures (MS) and subsequently coated them with a hydrophobic coating with candle soot (top) or OTS solution (bottom) for 10 mins. The inset on the right shows the microscope (top-view) image of the 3D printed microstructures after a hydrophobic coating. The scale bar corresponds to 500 μm.

composition of the material or creating efficient micro- or nanoscale structures to fabricate robust SH structures. The effect of micro- or nanoscale structures on surface wetting is commonly attributed to two wetting modes: first, homogeneous Wenzel (W) wetting state, where the liquid fills in the surface cavities and completely wets the surface textures,[16] and second, heterogeneous wetting of Cassie-Baxter (CB) mode, in which the liquid drop sits on the top of the hydrophobic texture with gas trapped beneath the drop.[17] The gas-trapping CB wetting state, contributing to a large contact angle and a low CA hysteresis, is critical to resilient superhydrophobicity, which is beneficial for various applications in surface engineering. However, the long-term stability of the preferred CB state on SH surfaces is still challenging and can be lost through an irreversible wetting transition to Wenzel state, when exposed to a high-temperature environment,[18] droplet evaporation,[19,20] or surfactant additives.[21–23]

In so far, numerous efforts have been made in fabricating artificial robust hydrophobic or SH surfaces using several micromachining technologies, including lithography,[24] chemical etching,[25] deep reactive-ion etching (DRIE),[26] polymer coating,[27] replica molding,[28] self-assembly,[29,30] electrospinning,[31] and so forth. These techniques are able to fabricate mostly two-dimensional (2D) patterns or 3D random structures or random roughness, unless using costly or multiple masks with specific geometries or simple 3D structures.[32–34] Albeit some studies reported complex 3D structures, their fabrication process is rather complicated, time-consuming, and expensive.[35,36]

Additive manufacturing (or 3D-printing technology) has recently attracted much interest because it can produce 3D structures with well-defined geometries on both rigid and flexible substrates via a one-step process and also utilize a wide variety of resin materials.[37,38] Besides, aiming at large-scale applications of superhydrophobic (or hybrid) surfaces, a few promising methods have been put forward lately, despite multiple chemical/material

engineering processes involved. Han et al.[39] used 3D-printed waveform microstructures to fabricate biomimetic hybrid (hydrophilic/hydrophobic) surfaces for water harvesting. This method involves multiple processes, including 3D-printing, solvent etching, mixture molding, and finally, hydrophilic sputtering to create nano/micro-roughness, resulting in a water contact angle of 136°. Liao et al.[40] fabricated a superhydrophobic conductive cotton fabric (of PDMS@AgNWs) in a size of 3 cm × 3 cm via a dipping-thermal curing method. The result yielded a high water contact angle of 156° and a good separation efficiency (of 95.6%) for an oil-water mixture. Wang et al.[41] developed highly hydrophobic composite coatings, by adding spherical and ellipsoid potato starch granules into PDMS solution that will be cured using a hot air gun for fifteen minutes. The obtained PDMS@starch composite coating has a water contact angle close to 150° and can separate an oil-water mixture, with the separation efficiency above 99% and a flux as high as 9460 L/m2 /h. Although a few of studies have lately demonstrated that a 3D-printing technology is effective in manufacturing SH surfaces,[42–54] there are still some challenges in the fabrication of resilient SH surfaces due to their short-term wetting stability or some additional complicated steps involved in the fabrication.

Here, we report facile and simple (one- and two-step) approaches to fabricate SH surfaces with a high CA and low roll-off angle (ROA) for self-cleaning and water-repellent applications (see Fig. 1). Using the one-step method, we are able to produce transparent superhydrophobic (TSH) surfaces with random roughness, to study the influence of random structures vs. regular patterns on the wetting properties and contact angles of water droplets on the SH surfaces fabricated. In the two-step process, we incorporate a 3D-printing technique with a hydrophobic coating to produce robust SH textures composed of regular square pillars, which are designed according to a thermodynamic theory for a stable gas-trapping CB state. Finally, our measurements of static and dynamic CAs of water droplets on all the prepared SH surfaces show high values and agree well with those predicted by using the Cassie–Baxter model.[17]

Material and Methods

Chemicals and devices

Polydimethylsiloxane (PDMS) (Sylgard184, Part A) with a curing agent (methylhydrosiloxane with Pt catalyst, Part B) was supplied by (Dow Corning Corporation). Microscope glass slides (GS, 26 mm × 76 mm × 1 mm) were purchased from (Bio Nuclear Diagnostics Inc) for the fabrication of the transparent SH surfaces. A muffle furnace (Thermo scientific) was used for the heat treatment process. Pyrex was used as a container for the PDMS during the heat treatment. Octadecyltrichlorosilane (OTS), toluene, sulfuric acid, hydrogen peroxide, acetone, and ethanol were obtained from Sigma-Aldrich Canada. Commercial candles were used for the hydrophobic coating of candle soot. All of the reagents were used as received without any further treatment. The water used in this experiment was ultra-pure Milli-Q water (PURELAB Ultra, resistivity: 18.2 MΩ.cm). 3D microstructured substrates were 3D printed with a clear resin using a 3D printer (Formlabs, Form 2).

One-Step Fabrication of Transparent Superhydrophobic Surfaces

A glass slide (GS) was used as the solid substrate, which was repeatedly and ultrasonically cleaned with acetone, ethanol, and rinsed with Milli-Q water several times, and finally dried using a nitrogen gun. The substrates were subsequently placed in a freshly prepared "piranha" solution,[55] a mixture of H_2SO_4/H_2O_2, 4:1 (v/v), for 1 h and rinsed several times with flowing Milli-Q water and finally dried with nitrogen. PDMS base and curing agent (at 10:1 mass ratio) were poured and mixed in a pyrex container for 10 mins. The mixture was then degassed in a vacuum desiccator until all the air bubbles were removed. The GS subsequently was placed upside down on the top of the pyrex, which contained the PDMS solution and was heated in a muffle furnace at 350°C for 4 hours. The distance between the PDMS liquid and the GS, as shown in Fig. 1a, was about 1.5 cm. After the heat treatment (350° for 4 h), the liquid PDMS decomposed and generated soot, which in turn de-

posited on the upper GS, forming a transparent SH surface[56] (see Fig. 2a). The surface coated with PDMS soot had an average static water contact angle of $\theta \simeq 170 \pm 2°$, as shown by the side-view in Fig 2a. The remaining white silicon powder left in the pyrex also shows super-repellency against water.

Two-Step Fabrication Processes of 3D-printed Superhydrophobic microstructures

To obtain SH microtextures, we designed our surfaces to have regular micron-sized square pillars of width, D, height, h, and interspace, S, in a square lattice with a periodicity, $P = D+S$ (see Fig. 2b-c). The microstructures were characterized with two crucial geometrical parameters: solid-liquid packing fraction, ϕ, which is the ratio of the liquid-solid surface area (pillar-top area) to the total (liquid-solid and liquid-gas) areas, and surface roughness, r, corresponding to the ratio of the total surface area to the projected one (on a 2D plane). These parameters can be calculated using the following relations:[59,60]

$$\phi = \frac{D^2}{P^2}, \tag{1}$$

$$r = \frac{P^2 + 4Dh}{P^2}. \tag{2}$$

Generally, r describes the relative change in the liquid/solid area for a rough surface compared to a flat surface in a Wenzel state.[16] ϕ describes the percentage of the liquid-solid contact area in a CB mode.[17]

To design SH surfaces with a stable CB state, we use a model based on the comparison of the global surface energies, E_{CB} and E_{W}, for a CB and the Wenzel wetting droplet on the microstructures, respectively. The total surface energy E_{CB} or E_{W} is the magnitude of the total energies needed for creating interfaces when placing a CB or Wenzel drop onto the microstructures. The total surface energy for a CB or a Wenzel droplet on the 3D-printed micro-texture, denoted by E_{CB} and E_W, respectively, can be modeled by:[1,19,55,58,61]

$$\begin{aligned} E_{\mathrm{CB}} = \; & N\,[\gamma_{\mathrm{ls}} D^2 + \gamma_{\mathrm{sg}}(4Dh + P^2 - D^2) \\ & + \; \gamma_{\mathrm{lg}}(P^2 - D^2)] + \gamma_{\mathrm{lg}} S_{\mathrm{cap}}, \end{aligned} \tag{3}$$

$$E_{\mathrm{W}} = N\,[\gamma_{\mathrm{ls}}(P^2 + 4Dh)] + \gamma_{\mathrm{lg}} S_{\mathrm{cap}}, \tag{4}$$

where $N = \frac{S_{\mathrm{b}}}{P^2}$ is the number of asperities beneath the drop, γ_{ls}, γ_{sg}, and γ_{lg} are the interfacial tensions for the liquid-solid, solid-gas, and liquid-gas interfaces, respectively, S_{cap} is the spherical cap surface area of the water drop entirely in contact with the air, and S_{b} is the base surface area. Here, we assume flat menisci beneath the drop. Using the Young–Duprè equation,[62] $\gamma_{\mathrm{ls}} = \gamma_{\mathrm{sg}} - \gamma_{\mathrm{lg}} \cos\theta_{\mathrm{Y}}$, the total surface energies for the two states on the superhydrophobic microstructures can be calculated using the roughness, r, and the solid fraction, ϕ:

$$E_{\mathrm{CB}} = \; S_{\mathrm{b}}\,[\gamma_{\mathrm{sg}} r + \gamma_{\mathrm{lg}}(1 - \phi\,(1 + \cos\theta_{\mathrm{Y}}))] + \gamma_{\mathrm{lg}} S_{\mathrm{cap}}\,, \tag{5}$$

$$E_{\mathrm{W}} = S_{\mathrm{b}}\,[\gamma_{\mathrm{sg}} r - \gamma_{\mathrm{lg}} r \cos\theta_{\mathrm{Y}}] + \gamma_{\mathrm{lg}} S_{\mathrm{cap}}. \tag{6}$$

The energy difference, $E_{CB} - E_W$, allows us to predict the critical contact angle θ^* when $E_{CB} = E_W$. Using the above two equations, one can arrive at the physical criterion of the critical contact angle θ^* that delineates the surface parameters for a stable CB vs. Wenzel state, by equating $E_{\mathrm{CB}} = E_{\mathrm{W}}$:[1,19,55,58,61]

$$\cos\theta^* = \frac{\phi - 1}{r - \phi}. \tag{7}$$

Theoretically, a CB droplet is thermodynamically more stable when $E_{CB} < E_W$, which corresponds to a larger contact angle, $\theta > \theta^*$. According to thermodynamics, a stable CB occurs when E_{CB} has a lower energy compared to that of a W wetting mode, i.e., $E_{CB} < E_W$, by tuning the surface parameters of r and ϕ.

This criterion is plotted in Fig. 2d. For the given important surface properties of r, ϕ, and θ_{F}, which is Young's contact angle of a water droplet on the flat surface of the same material, a stable CB state can occur on the hydrophobic micro-structures with a high roughness $r > (\phi - 1)/\cos\theta_{\mathrm{F}} + \phi$ (i.e., the upper (yellow) area in Fig. 2 d). Based

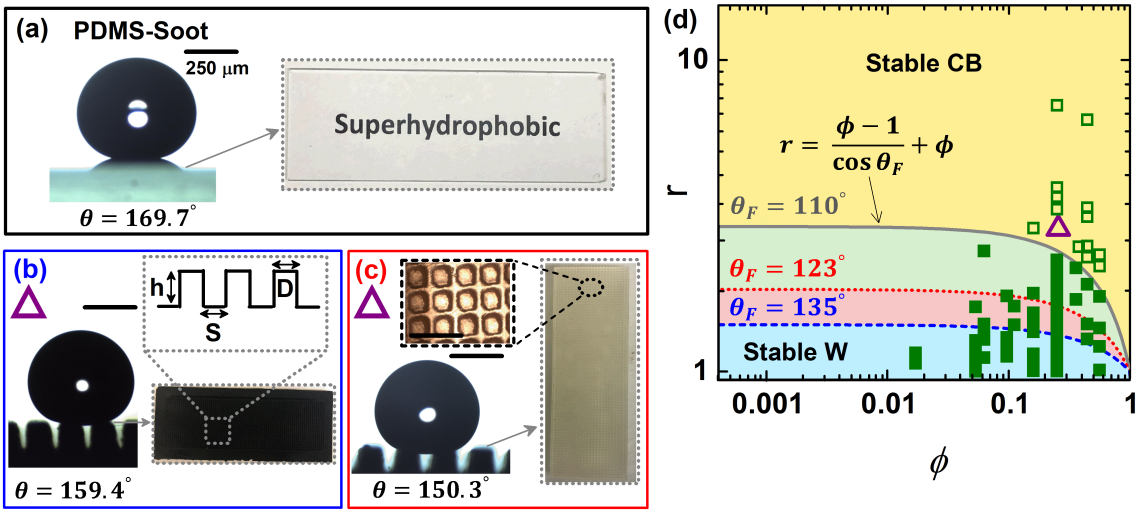

Figure 2. (a) Side-view of a water droplet deposited on the transparent PDMS-soot SH surface fabricated, revealing a Cassie-Baxter (CB) wetting state with an extremely high contact angle of $\theta = 169.7°$. Side-view of a water droplet deposited on the 3D-printed microstructures coated with candle soot (CS) in (b), while with OTS in (c). After the hydrophobic coating, the additive manufactured microtextures become superhydrophobic (SH) with a large contact angle ($\theta > 150°$), revealing a gas-trapping CB wetting state for a water droplet. The insets in (b) and (c) show the top-view of the SH micro-structures fabricated. The microtextures are 3D-printed with a square pillar pattern of pillar width (D), height (h), and separation distance (S), which are designed according to a thermodynamic theory to have a stable CB wetting state. Here, D, h, and S are of the order of magnitude of 10^{-4}m, yielding the surface roughness and packing fraction to be $r = 2.87$ and $\phi = 0.27$, respectively. The small inset in (c) shows an optical microscopic image of the top-view of the superhydrophobic surface coated with OTS (△). The scale bars in (b) and (c) correspond to 500 μm. (d) Phase diagram based on the energetic argument[55,57,58] can be divided into a stable CB state region (in the upper region, e.g., yellow) and a stable W phase (in the lower region, e.g., green, pink, and blue) for different Young's angles (θ_F). For a comparison, we also plot previous experimental data by Yeh and Chen using square-pillar microstructures[59] (with □, ■, denoting a CB and Wenzel state, respectively). The critical CB-W separation lines based on Eq. (7) are plotted for different Young's contact angles on flat surfaces, for Yeh and Chen's OTS-coated surface with $\theta_F = 110°$[59] (——) as well as our surfaces coated with OTS of $\theta_F = 123°$ (·····) and with CS of $\theta_F = 135°$ (- - -). At high surface roughness (r) and high solid-fraction (ϕ), the initial drop shape always exhibits CB states (denoted by the open symbols △ & □), whereas a Wenzel state (denoted by the filled symbols ■) is more likely observed experimentally at low r and ϕ.

on the criterion above, we designed using SolidWorks and subsequently printed two microstructured substrates using a Formlabs (Form 2) 3D-printer. In our designs, considering the printing resolution of our 3D printer, the microstructures are printed in an area size of 66 mm × 20 mm, with square-shaped micropillars of $h = 750$ μm, $D = 410$ μm, and $S = 400$ μm. The printing time for every two identical substrates was around 8 hours. The corresponding surface parameters, according to eqs. (1)–(2), are $r = 2.87$ and $\phi = 0.27$, indicated by the symbol (△) in Fig. 2 d, and theoretically a stable CB wetting is expected for a water droplet on the SH microstructured fabricated.

We experimentally measured the contact angles of a water droplet on the flat 3D-printed surfaces coated with candle soot and OTS to be 135° and 123°, respectively, so as to estimate θ_F for these materials. With these values of θ_F measured, using eq. (7), we plot the critical criteria for the different θ_F-values in Fig. 2d. Based on the thermodynamic model, a stable CB drop occurs in the upper region above the critical criterion (i.e., higher r), whereas a Wenzel state is more favorable for low-roughness surfaces (i.e., the grey, pink, and blue regions for different Young angles, θ_F) since $E_W < E_{CB}$. In a good agreement, we always observed a CB state of the initial drop on the SH substrates fabricated

with 3D printing since our microstructure design has $r = 2.87$ and $\phi = 0.27$, shown as (△) in Fig. 2d, which is located in the upper (yellow) region of a stable CB state (above the critical criterion boundary for the Young angle of interest, e.g., $\theta_F = 135°$ and 123°).

From the two 3D-printed microstructures, one of the printed substrates was subsequently coated with candle soot,[63–66] while the other with an OTS solution[67–69] to achieve super-repellent properties with a high contact angle. The former 3D-printed microstructured substrate was brought horizontally over the center of the candle flame upside down and moved across back and forth for 10 mins until the substrate became black to obtain a uniform layer of soot deposition (see Fig. 1b for the schematic procedure). The substrate treated with candle soot, shown in Fig. 2b, had an average static water contact angle of $\theta \simeq 158 \pm 2°$.

The second microstructure was dipped into an OTS/toluene solution (0.2 ml of OTS into 100 ml of toluene, 0.2 vol%) for 10 mins to allow the OTS to uniformly deposit on the sample (see Fig. 1c for the illustration). Substrate modified with OTS was cleaned by sonication in toluene and by rinsing again with toluene, ethanol, and Milli-Q water several times, and finally dried with nitrogen. The surface treated with OTS, shown in Fig. 2c, had an average static water contact angle of $\theta \simeq 147 \pm 2°$.

Characterization

The surface morphologies of the as-fabricated transparent PDMS-soot glass substrates were observed with field-emission scanning electron microscopy (FESEM, Zeiss Sigma), at an acceleration voltage of 5 kV and at different magnifications, ranges from 1k to 99k x. From the SEM images, shown in Fig.3e-f, the deposition layers are shown to be a large number of micron-sized clusters, with sizes ranging from 200 nm to 1 μm, while nanosized shoot particles of O(10 nm) are coated on the clusters. As illustrated in the high-magnification SEM images, each cluster displays nanowrinkle structures, forming multi-scale roughness of TSH surface on the glass substrate. Both roughness and low-surface-energy are vital for ultra-hydrophobicity. Herein, PDMS solution and nanoscale wrinkles were beneficial to the hierarchical structure, and PDMS can reduce surface energy for fabricating ultra-hydrophobic coatings.

Fourier transform infrared spectroscopy (FT-IR) measurements were carried out for the plain glass and the PDMS-soot coating using an FT-IR spectrometer (Nicolet 8700) to examine the SH sample transparency. The transmittance data of the PDMS-soot coated glass was close to 80% for wavenumber ranging from 2500 – 4000 cm^{-1}, maintaining their optical transparency, when compared with the plain glass.

Results and Discussion

Wetting State and Contact Angle Measurements

The wettability of both the TSH and the 3D-printed SH microstructures (shown in Fig. 2) is characterized using static water CA, dynamic CA (in terms of the advancing and receding CAs), and the ROA. The roll-off angle (ROA) or so-called "the angle of inclination" is the minimum tilting angle at which a water drop rolls off a tilted SH surface. The ROA is measured experimentally using a movable stage (Thorlabs TTR001), which allows for accurately tilting from its initial horizontal position to an inclined position. While still horizontal, a 10 μl Milli-Q water droplet was gently deposited on the testing surface, after which the stage was slowly tilted until this droplet began to roll over the surface. At this point, the stage angle relative to the horizontal was measured and recorded. This measurement was performed at least seven times for each sample, and all reported ROAs are averages of all measurements.

On the one hand, static water droplet CAs on the TSH surface with random roughness showed a greater contact angle with $\theta \simeq 170 \pm 2°$. On the other, the static CA on the 3D-printed SH microstructures coated with CS and OTS were smaller, with $\theta \simeq 158 \pm 2°$ and $\theta \simeq 147 \pm 2°$, respectively. All these fabricated substrates were superhydrophobic, i.e., $\theta \geq 150°$ as shown in Fig. 4. From Fig. 4a-b, we can clearly see the trapped air between the surface microstructures underneath the drop. Since both the 3D-printed microstructured SH surfaces have the same surface structure

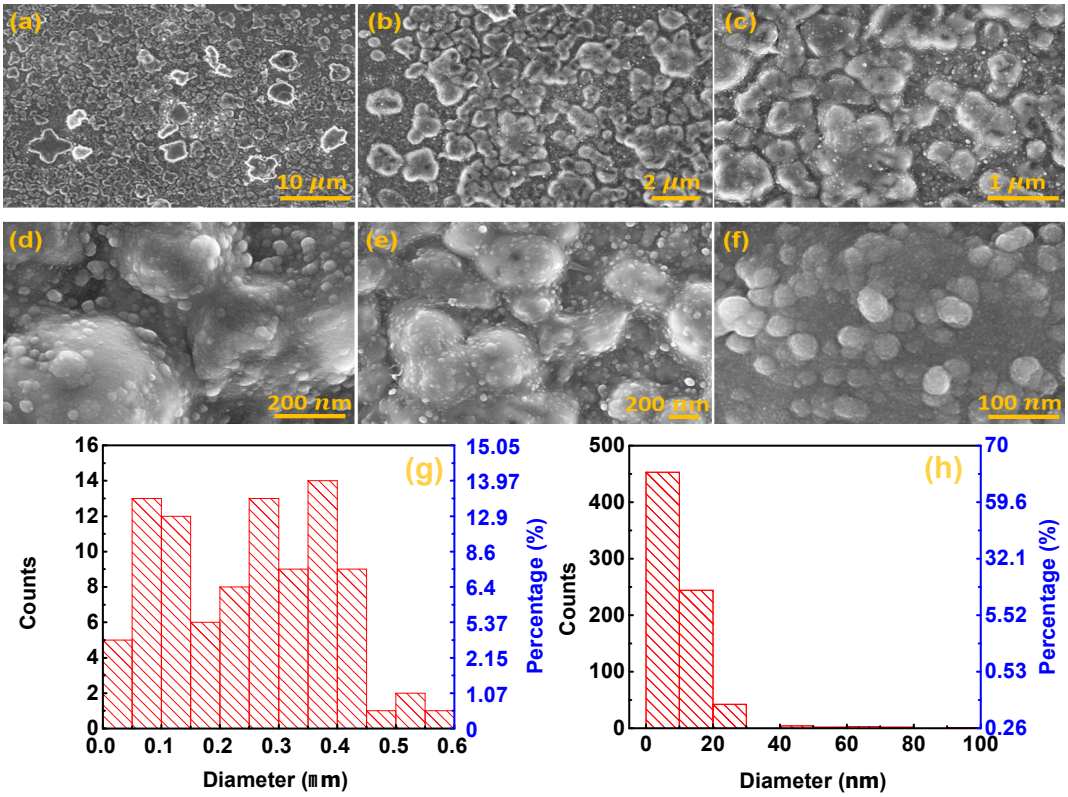

Figure 3. SEM images of the transparent PDMS-soot glass substrates at different magnifications: (a) 1k, (b) 5k, (c) 10k, (e) 20k, and (d) 50k, (f) 99k × of magnification. (g) and (h) are the cluster/particle size distributions of the SEM images in (b) and (f), respectively. The total numbers of counts in (b) and (f) are 296 and 760, respectively.

($\phi = 0.27$ & $r = 2.87$) but have different static water droplet CA (by $\approx 10°$), revealing that not only the surface pattern but also the coating chemical composition can alter the SH CA on the surfaces.

Two classical models have been used to describe surface wettability in terms of surface roughness r and solid-liquid contact area ϕ: Cassie-Baxter (CB) and Wenzel (W) models. In a CB state, the surface structure assumed to be partially wetted by the liquid. In this case, the liquid droplet is in contact with the top of the surface pattern, while a thin air layer is trapped beneath the drop. Surface texture, in the later, is assumed to be completely wetted with liquid in a W state. The contact angle for each model is formulated as follows:[16,17]

$$\cos\theta_{CB} = \phi\cos\theta_F - (1-\phi), \tag{8}$$

$$\cos\theta_W = r\cos\theta_F, \tag{9}$$

where θ_{CB} is the CA of water droplets on a rough surface in a CB state, ϕ, as defined earlier, is the solid-liquid area fraction to the projected area, θ_F is the Young CA of a water droplet on a smooth, flat, rigid, homogeneous, and chemically inert surface, θ_W is the CA of water droplets on a rough surface in a W state, and r is the surface roughness factor.

To compare with our experimental data, static water droplet CAs are then theoretically estimated using the CB equation (8) and the Young CAs on the flat GS as well as the flat 3D-printed surfaces coated with OTS and CS, i.e., $\theta_F \approx 35°$, 123° and 135°, respectively. As shown in Fig. 5a, the experimental CAs agree well with the CAs modeled by the CB equation (8), revealing that all the studied surfaces wetted in a CB mode with air trapped beneath the drop. Since the valid range of the cosine function is between -1 and 1 and the multiplication of the terms ($r\cos\theta_F$) is either < -1 or > 1, the Wenzel equation is not applicable in our case.

In addition to the static water droplet CA, the dynamic CAs (i.e., advancing and receding CAs) and ROAs are measured to evaluate the surface adhesion. Fig. 5 b-c shows water droplet advancing and receding CAs on the three types of SH surfaces fabricated. The average advancing CA and the

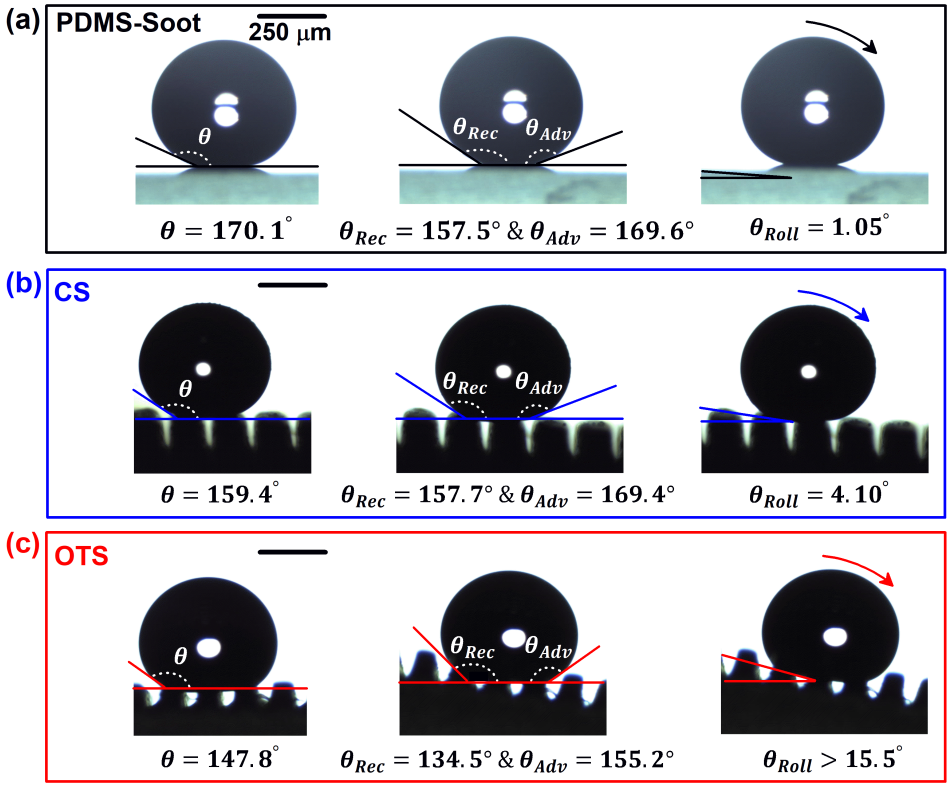

Figure 4. Comparison of water droplet static, dynamic (in terms of advancing and receding), and roll-off contact angles on (a) Glass substrate coated with PDMS-soot, (b) 3D-printed microstructures (r = 2.87, ϕ = 0.27) coated with candle soot (CS), and (c) 3D-printed microstructures coated with OTS. Both the glass coated with PDMS-soot and the CS microstructured SH surfaces show a high static contact angle and a low roll-off angle, $\theta_{Roll} < 5°$.

standard deviation of seven water droplets on the TSH surface was about $\theta_{\text{Adv}} \simeq 168.9 \pm 1.4°$, which is close to that on the 3D-microstructured surface coated with CS, $\theta_{\text{Adv}} \simeq 167.4 \pm 2.5°$. While the advancing CA on the 3D-microstructured surface coated with OTS was around $\theta_{\text{Adv}} \simeq 154.3 \pm 2.6°$, which is lower than the former by approximately 13°. The average receding CAs were also measured to be large, as illustrated in Fig. 4 and Fig. 5c.

The measured advancing and receding CAs of water droplets on the studied surfaces were consistent with the theoretical prediction using the CB equation due to the presence of air pockets between water droplets and surface cavities. We determined the contact angle hysteresis (CAH), which is the difference between the advancing and receding contact angles. The average CAH values (with the standard deviation of seven water droplets) are $\theta_{CAH} \approx 11° (\pm 3°)$, $10° (\pm 2°)$, $17° (\pm 4°)$ and on the TSH, 3D microstructures coated with CS, and 3D-microtextures coated with OTS, respectively. Furthermore, the ROAs of both the 3D-printed microstructured surface coated with CS and the GS surface coated with PDMS-soot were extremely low, $\theta_{Roll} \lesssim 5°$, which makes them great candidates for self-cleaning and water repellent applications. The 3D-printed microstructures coated with OTS, however, showed a higher ROA of approximately $\theta_{Roll} > 15°$, which makes the droplet adhere more to the surface.

Chemical and Mechanical Stability of the SH Surfaces

Superhydrophobic surfaces' longevity and stability are vital for their applications in practice, as some rough micro/nanostructures required in fabricating superhydrophobic surfaces may be too fragile to resist chemical and mechanical damages. Therefore, we further investigated the superhydrophobic substrates' chemical and mechanical stability under severe circumstances, including exposing them to different chemicals and mechanical

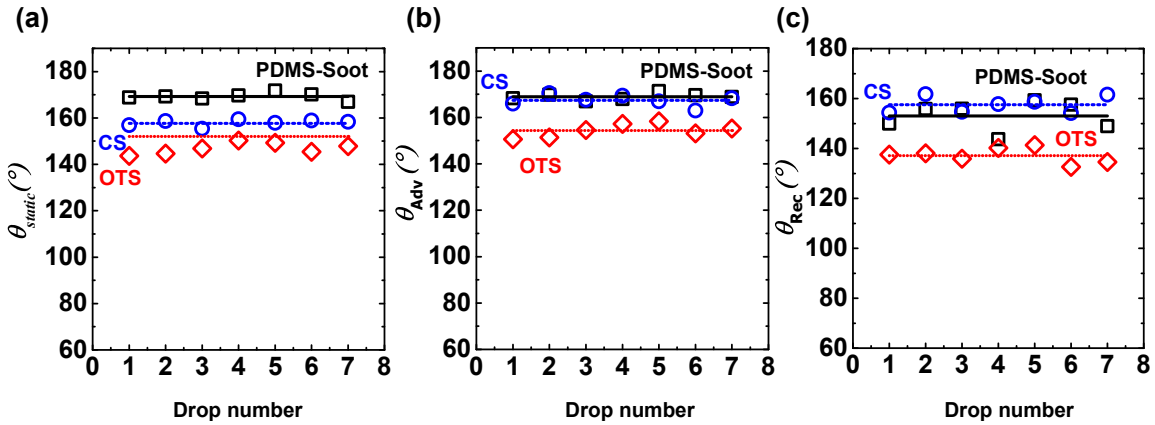

Figure 5. Comparison of measured static water droplet CA in (a) and dynamic CAs (in terms of advancing (b) and receding (c)) with Cassie-Baxter theoretical model on glass substrate coated with PDMS-soot (□,—), 3D-printed microstructures (r = 2.87, ϕ = 0.27) coated with candle soot (CS) (◯,- - -), and 3D-printed microstructures coated with OTS (◇,·····) for seven drops on different spots on each surface.

ultrasonic vibration.

First, we conducted the surfaces' chemical stability by exposing all three surfaces to 6 different solvents such as acetone, poly(diallyldimethylammonium chloride) solution (PDADMAC), hexadecane, hexane, propylene glycol, and acetic acid. All of the reagents were obtained from Sigma-Aldrich Canada and used as received without any further treatment. Shown in Fig. 6 are the additional measurements of static CAs for various droplets of different chemicals on the SH surfaces. From all the CA data, both the PDMS-soot and the 3D-microstructured CS surfaces still retain superior superhydrophobicity towards water and all the used solvents, except the OTS-coated surface lost its super-repellency toward hexadecane, hexane, propylene glycol, acetic acid with a moderate CA decrease.

Next, we examined our SH surfaces' mechanical stability since, for some applications, superhydrophobic coatings may degrade when working under aqueous solutions with turbulent flow. Therefore, we performed a harsh underwater ultrasonication test to evaluate the mechanical stability of the studied surfaces. Herein, all the three superhydrophobic coatings were directly immersed into Milli-Q water, treated with 20 kHz ultrasonication for a different amount of time, ranges from 0 to 60 minutes. All samples were dried using a nitrogen gun before contact angle measurements. As shown in Fig. 7, the static water CAs of the

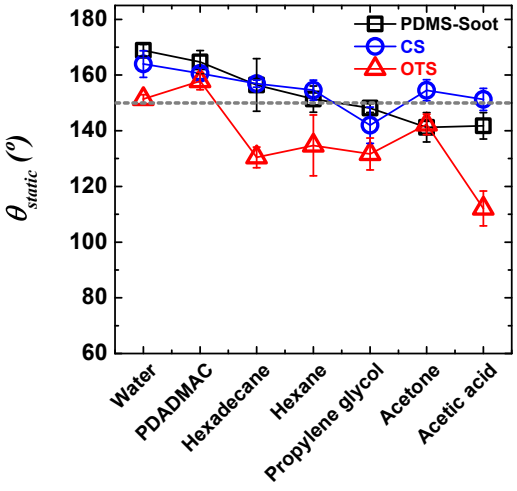

Figure 6. Comparison of the measured static CA for various liquids on glass substrate coated with PDMS-soot (□,—), 3D-printed microstructures (r = 2.87, ϕ = 0.27) coated with candle soot (CS) (◯,—), and 3D-printed microstructures coated with OTS (△,—) for five drops on different spots on each surface.

PDMS-soot, candle soot, and OTS coatings decreased to about 158°, 153°, 143°, respectively, after ultrasonication treatment for 60 minutes. The results suggest that the top loose coating layer may be dissolved/removed in water. At the same time, the remaining firmly attached part to the substrate showed superhydrophobic properties with high water contact angle, especially for PDMS-soot and candle soot. Based on the stability test results, these SH surfaces/coatings reveal an excellent candidate for self-cleaning and underwater

turbulent drag reduction applications.

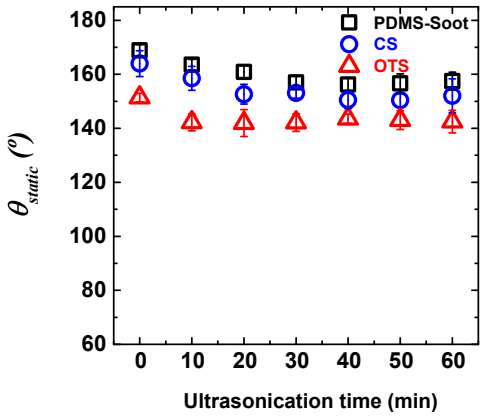

Figure 7. Mechanical stability of the superhydrophobic surfaces (in terms of static water CA) against a ultrasonication treatment for different durations. Comparison of the measured static CA on glass substrate coated with PDMS-soot (□), 3D-printed microstructures ($r = 2.87$, $\phi = 0.27$) coated with candle soot (CS) (◯), and 3D-printed microstructures coated with OTS (△) for five drops on different spots on each surface.

Moreover, to test the longevity of the SH surfaces against the air-exposure time, we conducted more measurements of static contact angles (SCAs) on the three studied surfaces at different time slots, ranging from an hour after surface preparation (0 days) to after being placed in the lab for 12 months (≈ 365 days). Even after one year since the fabrication, these samples (kept in a petridish) still show good superhydrophobicity with their CAs slightly decrease from averagely 170°, 164°, 156° to 167°, 158°, 147° (by ≈ 3°, 6°, 9°) for the glass substrate coated with PDMS-soot, 3D-printed microstructures coated with candle soot (CS) and coated with OTS, respectively.

Some recent studies reported facile methods that are applicable for large-scale fabrications of hybrid or superhydrophobic materials for the applications of water harvesting,[39] oil-water separation, quick deicing,[40] piezoresistive sensing for human motion,[40] and oil-water separation.[41] These methods used PDMS in a liquid state by either pour it onto a 3D-printed mold[39] or mix it with nanoparticles[40,41] and usually involve multiple chemical and material engineering processes. In comparison, our methods yield more robust superhydrophobicity with a water CA of 160° on average,

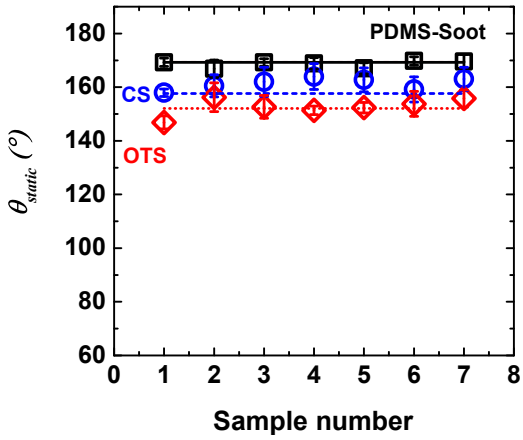

Figure 8. Comparison of the measured static water droplet CA and Cassie-Baxter theoretical model on glass substrate coated with PDMS-soot (□,▬), 3D-printed microstructures ($r = 2.87$, $\phi = 0.27$) coated with candle soot (CS) (◯,- - -), and 3D-printed microstructures coated with OTS (◇,·····) for seven different samples. The error bar represents the standard deviation of seven droplets on each surface.

while possessing long-term material and mechanical stability.

Method Reproducibility for Mass Production

For the tests of reproducibility and mass production, six more samples were fabricated and evaluated by measuring the static, dynamic (in terms of the advancing and receding) CAs, and ROAs (the static CA showed in Fig. 8). All the samples showed superhydrophobic behavior with a large CA and a low ROA, and the results agree well with the previous ones. From the agreeable results of the seven samples, we confirmed the reproducibility of these methods to obtain robust SH surfaces that can be mass production using a 3D printing technology. These superhydrophobic surfaces fabricated enable a stable CB wetting for a water droplet and can benefit various applications such as self-cleaning and drag-reduction.

Conclusions

In summary, superhydrophobic surfaces are facilely obtained using simple one and two-step fabricating processes. For the former, a transparent SH surface was created via an only single heating process of PDMS at 350° for 4 h, by depositing PDMS-soot on the GS. The surface obtained using this method showed great superhydrophobicity and super-repellency properties with an ultrahigh CA and ultra-low ROA. The latter, two-step method was composed of, first, 3D-printed microstructured surface and, second, a hydrophobic coating using either CS or OTS. The 3D-printed microstructures coated with CS showed better superhydrophobic properties with a high static water CA and low ROA, compared to those with OTS coating. This reveals that additional nano-roughness from the candle shoot (on top of hydrophobic MS) enhances the non-wetting property or superhydrophobicity greatly.

In terms of applications, a water droplet exhibits a spherical shape on the GS coated with PDMS-soot and 3D-printed CS surfaces, which can be easily rolled-off by incline the surface few degrees to remove dirt or contaminants in their way. Our SH surfaces possess robust superhydrophobicity against the various chemical droplets tested, a ultrasonic treatment in water bath (for 1 hr), and at least one-year-long shelf life. Finally, we provide here promising facile, cost-effective, and highly efficient fabrication strategies for preparing transparent super-repellent and superhydrophobic surfaces using a 3D-printing technique by incorporating a thermodynamic model. The method provided is capable of a large-scale production and can be applied widely in the applications of self-cleaning and super-repellent materials in the fields of surface engineering and material.

Acknowledgement AA and PAT acknowledges funding from Natural Sciences and Engineering Research Council of Canada (NSERC) and Alberta Innovate (AI). PAT holds a Canada Research Chair in Fluids and Interfaces.

References

(1) Quéré, D. Non-sticking drops. Rep. Prog. Phys. **2005**, 68, 2495–2532.

(2) Jiang, L.; Zhao, Y.; Zhai, J. A lotus-leaf-like superhydrophobic surface: a porous microsphere/nanofiber composite film prepared by electrohydrodynamics. Angew.Chem.Int.Ed. **2004**, 43, 4338–4341.

(3) Yuan, Z.; Chen, H.; Zhang, J. Facile method to prepare lotus-leaf-like super-hydrophobic poly (vinyl chloride) film. Appl. Surf. Sci. **2008**, 254, 1593–1598.

(4) Zorba, V.; Stratakis, E.; Barberoglou, M.; Spanakis, E.; Tzanetakis, P.; Anastasiadis, S. H.; Fotakis, C. Biomimetic artificial surfaces quantitatively reproduce the water repellency of a lotus leaf. Adv. Mater. **2008**, 20, 4049–4054.

(5) Ma, M.; Gupta, M.; Li, Z.; Zhai, L.; Gleason, K. K.; Cohen, R. E.; Rubner, M. F.; Rutledge, G. C. Decorated electrospun fibers exhibiting superhydrophobicity. Adv. Mater. **2007**, 19, 255–259.

(6) Feng, L.; Li, S.; Li, Y.; Li, H.; Zhang, L.; Zhai, J.; Song, Y.; Liu, B.; Jiang, L.; Zhu, D. Super-hydrophobic surfaces: from natural to artificial. Adv. Mater. **2002**, 14, 1857–1860.

(7) Zheng, Y.; Gao, X.; Jiang, L. Directional adhesion of superhydrophobic butterfly wings. Soft Matter **2007**, 3, 178–182.

(8) Lai, Y.; Tang, Y.; Gong, J.; Gong, D.; Chi, L.; Lin, C.; Chen, Z. Transparent superhydrophobic/superhydrophilic TiO 2-based coatings for self-cleaning and anti-fogging. J. Mater. Chem. **2012**, 22, 7420–7426.

(9) Liu, Y.; Chen, J.; Guo, D.; Cao, M.; Jiang, L. Floatable, self-cleaning, and carbon-black-based superhydrophobic gauze for the solar evaporation enhancement at the air–water interface. ACS Appl. Mater. Interfaces **2015**, 7, 13645–13652.

(10) Bagheri, H.; Aliofkhazraei, M.; Forooshani, H. M.; Rouhaghdam, A. S. Electrodeposition of the hierarchical dual structured (HDS) nanocrystalline Ni surface with high water repellency and self-cleaning properties. JJ. Taiwan Inst. Chem. Eng. **2017**, 80, 883–893.

(11) Cao, L.; Price, T. P.; Weiss, M.; Gao, D. Super water-and oil-repellent surfaces on intrinsically hydrophilic and oleophilic porous silicon films. Langmuir **2008**, 24, 1640–1643.
(12) Zhang, W.; Shi, Z.; Zhang, F.; Liu, X.; Jin, J.; Jiang, L. Superhydrophobic and superoleophilic PVDF membranes for effective separation of water-in-oil emulsions with high flux. Adv. Mater. **2013**, 25, 2071–2076.
(13) Daniello, R. J.; Waterhouse, N. E.; Rothstein, J. P. Drag reduction in turbulent flows over superhydrophobic surfaces. Phys. Fluids **2009**, 21, 085103.
(14) Kreder, M. J.; Alvarenga, J.; Kim, P.; Aizenberg, J. Design of anti-icing surfaces: smooth, textured or slippery? Nat. Rev. Mater. **2016**, 1, 1–15.
(15) Xue, C.-H.; Guo, X.-J.; Ma, J.-Z.; Jia, S.-T. Fabrication of robust and antifouling superhydrophobic surfaces via surface-initiated atom transfer radical polymerization. ACS Appl. Mater. Interfaces **2015**, 7, 8251–8259.
(16) Wenzel, R. N. Resistance of solid surfaces to wetting by water. Ind. Eng. Chem. **1936**, 28, 988–994.
(17) Cassie, A.; Baxter, S. Wettability of porous surfaces. J. Chem. Soc. Faraday Trans. **1944**, 40, 546–551.
(18) Shirtcliffe, N. J.; McHale, G.; Newton, M. I.; Perry, C. C.; Roach, P. Superhydrophobic to superhydrophilic transitions of sol–gel films for temperature, alcohol or surfactant measurement. Mater. Chem. Phys. **2007**, 103, 112–117.
(19) Tsai, P.; Lammertink, R. G.; Wessling, M.; Lohse, D. Evaporation-triggered wetting transition for water droplets upon hydrophobic microstructures. Phys. Rev. Lett. **2010**, 104, 2–3.
(20) Aldhaleai, A.; Khan, F.; Thundat, T.; Tsai, P. A. Evaporation dynamics of water droplets on superhydrophobic nanograss surfaces. Int. J. Heat Mass Transf. **2020**, 160, 120149.
(21) Chang, F.-M.; Sheng, Y.-J.; Chen, H.; Tsao, H.-K. From superhydrophobic to superhydrophilic surfaces tuned by surfactant solutions. Appl. Phys. Lett. **2007**, 91, 1–4.
(22) Shardt, N.; Bigdeli, M. B.; Elliott, J. A.; Tsai, P. A. How Surfactants Affect Droplet Wetting on Hydrophobic Microstructures. J. Phys. Chem. Lett. **2019**, 10, 7510–7515.
(23) Aldhaleai, A.; Tsai, P. A. Effect of a Cationic Surfactant on Droplet Wetting on Superhydrophobic Surfaces. Langmuir **2020**, 36, 4308–4316.
(24) Yang, Y.-L.; Hsu, C.-C.; Chang, T.-L.; Kuo, L.-S.; Chen, P.-H. Study on wetting properties of periodical nanopatterns by a combinative technique of photolithography and laser interference lithography. Appl. Surf. Sci. **2010**, 256, 3683–3687.
(25) Xiu, Y.; Liu, Y.; Hess, D. W.; Wong, C. Mechanically robust superhydrophobicity on hierarchically structured Si surfaces. Nanotechnology **2010**, 21, 155705.
(26) Kwon, Y.; Patankar, N.; Choi, J.; Lee, J. Design of surface hierarchy for extreme hydrophobicity. Langmuir **2009**, 25, 6129–6136.
(27) Levkin, P. A.; Svec, F.; Fréchet, J. M. Porous polymer coatings: a versatile approach to superhydrophobic surfaces. Adv. Funct. Mater. **2009**, 19, 1993–1998.
(28) Choi, S.-J.; Huh, S.-Y. Direct structuring of a biomimetic anti-reflective, self-cleaning surface for light harvesting in organic solar cells. Macromol. Rapid Commun. **2010**, 31, 539–544.
(29) Song, X.; Zhai, J.; Wang, Y.; Jiang, L. Fabrication of superhydrophobic surfaces by self-assembly and their water-adhesion properties. J. Phys. Chem. B **2005**, 109, 4048–4052.
(30) Pokroy, B.; Kang, S. H.; Mahadevan, L.; Aizenberg, J. Self-organization of a mesoscale bristle into ordered, hierarchical helical assemblies. Science **2009**, 323, 237–240.
(31) Sas, I.; Gorga, R. E.; Joines, J. A.; Thoney, K. A. Literature review on superhydrophobic self-cleaning surfaces produced by electrospinning. J Polym Sci B Polym Phys **2012**, 50, 824–845.
(32) Zhang, D.; Chen, F.; Yang, Q.; Si, J.; Hou, X. Mutual wetting transition between isotropic and anisotropic on directional structures fabricated by femotosecond laser. Soft Matter **2011**, 7, 8337–8342.

(33) Zhang, Z.; Yu, Y.; Wang, P. Hierarchical top-porous/bottom-tubular TiO2 nanostructures decorated with Pd nanoparticles for efficient photoelectrocatalytic decomposition of synergistic pollutants. ACS Appl. Mater. Interfaces **2012**, 4, 990–996.
(34) Feng, J.; Tuominen, M. T.; Rothstein, J. P. Hierarchical superhydrophobic surfaces fabricated by dual-scale electron-beam-lithography with well-ordered secondary nanostructures. Adv. Funct. Mater. **2011**, 21, 3715–3722.
(35) Yong, J.; Yang, Q.; Chen, F.; Zhang, D.; Du, G.; Bian, H.; Si, J.; Yun, F.; Hou, X. Superhydrophobic PDMS surfaces with three-dimensional (3D) pattern-dependent controllable adhesion. Appl. Surf. Sci. **2014**, 288, 579–583.
(36) Liu, Y.; Das, A.; Lin, Z.; Cooper, I. B.; Rohatgi, A.; Wong, C. Hierarchical robust textured structures for large scale self-cleaning black silicon solar cells. Nano Energy **2014**, 3, 127–133.
(37) Snyder, T. J.; Andrews, M.; Weislogel, M.; Moeck, P.; Stone-Sundberg, J.; Birkes, D.; Hoffert, M. P.; Lindeman, A.; Morrill, J.; Fercak, O.; Friedman, S.; Gunderson, J.; Ha, A.; McCollister, J.; Chen, Y.; Geile, J.; Wollman, A.; Attari, B.; Botnen, N.; Vuppuluri, V.; Shim, J.; Kaminsky, W.; Adams, D.; Graft, J. 3D systems' technology overview and new applications in manufacturing, engineering, science, and education. 3D Print Addit Manuf **2014**, 1, 169–176.
(38) Ngo, T. D.; Kashani, A.; Imbalzano, G.; Nguyen, K. T.; Hui, D. Additive manufacturing (3D printing): A review of materials, methods, applications and challenges. Compos. B. Eng. **2018**, 143, 172–196.
(39) Han, S.; Sung, J.; So, H. Simple Fabrication of Water Harvesting Surfaces Using Three-Dimensional Printing Technology. International Journal of Precision Engineering and Manufacturing-Green Technology **2020**, 1–11.
(40) Liao, X.; Li, H.; Lai, X.; Chen, W.; Zeng, X. Facile fabrication of superhydrophobic conductive polydimethylsiloxane@ silver nanowires cotton fabric via dipping-thermal curing method. Mater. Lett. **2019**, 255, 126511.
(41) Wang, Y.; Wang, M.; Wang, J.; Wang, H.; Men, X.; Zhang, Z. A rapid, facile and practical fabrication of robust PDMS@ starch coatings for oil-water separation. J Taiwan Inst Chem Eng **2019**, 99, 215–223.
(42) Lin, Y.; Zhou, R.; Xu, J. Superhydrophobic surfaces based on fractal and hierarchical microstructures using two-photon polymerization: toward flexible superhydrophobic films. Adv. Mater. Interfaces **2018**, 5, 1–8.
(43) Milionis, A.; Noyes, C.; Loth, E.; Bayer, I.; Lichtenberger, A.; Stathopoulos, V.; Vourdas, N. Water-repellent approaches for 3-D printed internal passages. Mater. Manuf. Processes **2016**, 31, 1162–1170.
(44) Yuan, S.; Zhu, J.; Li, Y.; Zhao, Y.; Li, J.; Van Puyvelde, P.; Van der Bruggen, B. Structure architecture of micro/nanoscale ZIF-L on a 3D printed membrane for a superhydrophobic and underwater superoleophobic surface. J. Mater. Chem. A **2019**, 7, 2723–2729.
(45) Yoon, H.-S.; Lee, H.-T.; Kim, E.-S.; Ahn, S.-H. Direct printing of anisotropic wetting patterns using aerodynamically focused nanoparticle (AFN) printing. Appl. Surf. Sci. **2017**, 396, 1450–1457.
(46) Graeber, G.; Martin Kieliger, O. B.; Schutzius, T. M.; Poulikakos, D. 3D-printed surface architecture enhancing superhydrophobicity and viscous droplet repellency. ACS Appl. Mater. Interfaces **2018**, 10, 43275–43281.
(47) Yang, Y.; Li, X.; Zheng, X.; Chen, Z.; Zhou, Q.; Chen, Y. 3D-printed biomimetic super-hydrophobic structure for microdroplet manipulation and oil/water separation. Adv. Mater. **2018**, 30, 1704912.
(48) Lee, K.-M.; Park, H.; Kim, J.; Chun, D.-M. Fabrication of a superhydrophobic surface using a fused deposition modeling (FDM) 3D printer with poly lactic acid (PLA) filament and dip coating with silica nanoparticles. Appl. Surf. Sci. **2019**, 467, 979–991.
(49) Yuan, S.; Strobbe, D.; Kruth, J.-P.; Van Puyvelde, P.; Van der Bruggen, B. Super-hydrophobic 3D printed polysulfone membranes with a switchable wettability

by self-assembled candle soot for efficient gravity-driven oil/water separation. J. Mater. Chem. A **2017**, 5, 25401–25409.
(50) He, Z.; Chen, Y.; Yang, J.; Tang, C.; Lv, J.; Liu, Y.; Mei, J.; Lau, W.-m.; Hui, D. Fabrication of Polydimethylsiloxane films with special surface wettability by 3D printing. Compos. B. Eng. **2017**, 129, 58–65.
(51) Lv, J.; Gong, Z.; He, Z.; Yang, J.; Chen, Y.; Tang, C.; Liu, Y.; Fan, M.; Lau, W.-M. 3D printing of a mechanically durable superhydrophobic porous membrane for oil–water separation. J. Mater. Chem. A **2017**, 5, 12435–12444.
(52) Wang, X.; Cai, X.; Guo, Q.; Zhang, T.; Kobe, B.; Yang, J. i3DP, a robust 3D printing approach enabling genetic post-printing surface modification. ChemComm **2013**, 49, 10064–10066.
(53) Koh, J. J.; Lim, G. J.; Zhou, X.; Zhang, X.; Ding, J.; He, C. 3D-Printed Anti-Fouling Cellulose Mesh for Highly Efficient Oil/Water Separation Applications. ACS Appl. Mater. Interfaces **2019**, 11, 13787–13795.
(54) Li, G.; Mo, X.; Wang, Y.; Chan, C.-Y.; Chan, K. C. All 3D-Printed Superhydrophobic/Oleophilic Membrane for Robotic Oil Recycling. Adv. Mater. Interfaces **2019**, 6, 1–5.
(55) Bussonnière, A.; Bigdeli, M. B.; Chueh, D.-Y.; Liu, Q.; Chen, P.; Tsai, P. A. Universal wetting transition of an evaporating water droplet on hydrophobic micro-and nanostructures. Soft matter **2017**, 13, 978–984.
(56) Long, M.; Peng, S.; Yang, X.; Deng, W.; Wen, N.; Miao, K.; Chen, G.; Miao, X.; Deng, W. One-step fabrication of non-fluorinated transparent super-repellent surfaces with tunable wettability functioning in both air and oil. ACS Appl. Mater. Interfaces **2017**, 9, 15857–15867.
(57) Bico, J.; Tordeux, C.; Quéré, D. Rough wetting. EPL **2001**, 55, 214–220.
(58) Ishino, C.; Okumura, K.; Quéré, D. Wetting transitions on rough surfaces. EPL **2004**, 68, 419–425.
(59) Yeh, K.-Y.; Chen, L.-J.; Chang, J.-Y. Contact angle hysteresis on regular pillar-like hydrophobic surfaces. Langmuir **2008**, 24, 245–251.
(60) Erbil, H. Y.; Cansoy, C. E. Range of applicability of the Wenzel and Cassie- Baxter equations for superhydrophobic surfaces. Langmuir **2009**, 25, 14135–14145.
(61) Gong, W.; Zu, Y.; Chen, S.; Yan, Y. Wetting transition energy curves for a droplet on a square-post patterned surface. Sci. Bull. **2017**, 62, 136–142.
(62) De Gennes, P.-G. Wetting: statics and dynamics. Rev. Mod. Phys. **1985**, 57, 827–863.
(63) Majhy, B.; Iqbal, R.; Sen, A. Facile fabrication and mechanistic understanding of a transparent reversible superhydrophobic–superhydrophilic surface. Sci. Rep. **2018**, 8, 1–11.
(64) Zhang, F.; Shi, Z.; Jiang, Y.; Xu, C.; Wu, Z.; Wang, Y.; Peng, C. Fabrication of transparent superhydrophobic glass with fibered-silica network. Appl. Surf. Sci. **2017**, 407, 526–531.
(65) Xiao, L.; Zeng, W.; Liao, G.; Yi, C.; Xu, Z. Thermally and chemically stable candle soot superhydrophobic surface with excellent self-cleaning properties in air and oil. ACS Appl. Nano Mater. **2018**, 1, 1204–1211.
(66) Iqbal, R.; Majhy, B.; Sen, A. Facile fabrication and characterization of a PDMS-derived candle soot coated stable biocompatible superhydrophobic and superhemophobic surface. ACS Appl. Mater. Interfaces **2017**, 9, 31170–31180.
(67) Lin, L.-Y.; Kim, H.-J.; Kim, D.-E. Wetting characteristics of ZnO smooth film and nanowire structure with and without OTS coating. Appl. Surf. Sci. **2008**, 254, 7370–7376.
(68) Song, Y.; Nair, R. P.; Zou, M.; Wang, Y. Adhesion and friction properties of micro/nano-engineered superhydrophobic/hydrophobic surfaces. Thin Solid Films **2010**, 518, 3801–3807.
(69) Yang, H.; Shin, K.; Tae, G.; Satija, S. K. Structure of a monolayer of poly (ethylene glycol) end-capped with a fluoroalkyl group and its relationship with protein adsorption at the aqueous interface. Soft matter **2009**, 5, 2731–2737.

Graphical TOC Entry